Ultrafast Science
A SCIENCE PARTNER JOURNAL

RESEARCH ARTICLE

Reconstructing Molecular Orbitals with Laser-Induced Electron Tunneling Spectroscopy

XuanYang Lai[1†], RenPing Sun[1†], ShaoGang Yu[1], YanLan Wang[1], Wei Quan[1], André Staudte[2*], and XiaoJun Liu[1*]

[1]State Key Laboratory of Magnetic Resonance and Atomic and Molecular Physics, Wuhan Institute of Physics and Mathematics, Innovation Academy for Precision Measurement Science and Technology, Chinese Academy of Sciences, Wuhan 430071, China. [2]Joint Attosecond Science Laboratory, National Research Council and University of Ottawa, Ottawa, Ontario K1A 0R6, Canada.

*Address correspondence to: andre.staudte@nrc-cnrc.gc.ca (A.S.); xjliu@wipm.ac.cn (X.L.)
†These authors contributed equally to this work.

Photoelectron spectroscopy in intense laser fields has proven to be a powerful tool for providing detailed insights into molecular structure. The ionizing molecular orbital, however, has not been reconstructed from the photoelectron spectra, because its phase information is difficult to access. Here, we propose a method to retrieve the phase information of the ionizing molecular orbital. By analyzing the interference pattern in the photoelectron spectrum, the weighted coefficients and the relative phases of the constituent atomic orbitals for a molecular orbital can be extracted. With this information, we reconstruct the highest occupied molecular orbital of N_2. Our work provides a reliable and straightforward approach for reconstructing molecular orbitals with the photoelectron spectroscopy.

Citation: Lai X, Sun R, Yu S, Wang Y, Quan W, Staudte A, Liu X. Reconstructing Molecular Orbitals with Laser-Induced Electron Tunneling Spectroscopy. *Ultrafast Sci.* 2024;4:Article 0038. https://doi.org/10.34133/ultrafastscience.0038

Submitted 11 July 2023
Accepted 4 October 2023
Published 5 January 2024

Introduction

Molecular orbital theory has been developed to describe the electronic structure of molecules [1] and has been extremely successful in explaining the chemical and physical properties of molecules. During the past decades, great progress has been made in developing imaging methods for molecular orbitals in real space using scanning tunneling microscopy [2,3], as well as in reciprocal space using photoemission spectroscopy [4–6]. The advance of high-repetition rate intense femtosecond lasers and single-electron imaging techniques enabled an alternative imaging scheme [7–12], which can trace the evolution of the molecular orbital with subfemtosecond resolution. In this scheme, which we call laser-induced electron tunneling spectroscopy (LETS), the outermost electron of a molecule can be ionized by tunneling through a barrier formed by the molecular potential and the laser electric field [13,14]. The ionized electron carries information of the molecular orbitals, which is imprinted in the observable molecular frame photoelectron angular distributions (PADs). Using this approach, the symmetry of the highest occupied molecular orbital (HOMO) of N_2 and O_2 has been directly observed [7]. By correlating fragmentation channels with the photoelectron spectra, this approach can be extended to image multiple contributing orbitals separately [15]. Furthermore, various intra- and intercycle interference patterns in the PADs are now well understood and separable [16], and can be exploited for reconstructing the ionizing orbital. Recently, LETS has clearly shown its inherent ability to image the real-time evolution of valence electron density [8]. However, until now, the molecular orbital has not been reconstructed with LETS. The main reason is that the phase information of the molecular orbital wavefunction, carried by the tunnel-ionized electron wavepacket, is erased during the detection of the photoelectron amplitudes.

In this work, we propose a LETS-based imaging method to completely reconstruct the molecular orbital, by extracting the weighted coefficients and the relative phases of its constituent atomic orbitals. According to molecular orbital theory, the molecular orbitals can be written as a linear combination of atomic orbitals (LCAO) [17,18]. For example, for the molecule N_2, the HOMO can be approximately written as a simple weighted sum of the 2*s* and 2*p* atomic orbitals. Such an approach has been also used for more complex biomolecules, e.g., DNA [19], using an orthogonalized LCAO theory. Within our imaging scheme, the tunnel-ionized electron wavepackets from the different constituent atomic orbitals in the framework of LCAO interfere with each other, causing a modulation in the PADs as illustrated in Fig. 1. By fitting the interference fringes in the PADs, the weighted coefficients and the relative phases of the different constituent atomic orbitals can be extracted. The retrieved coefficients and phases are used to reconstruct the molecular orbital with the corresponding atomic-orbital wavefunctions within the LCAO framework. We experimentally and theoretically identify the fingerprints of the different atomic orbitals in the PADs and show that they can be used to reconstruct the molecular orbital for the example of N_2.

It is worth noting that our molecular-orbital imaging scheme is different from the tomographic orbital imaging with high-order

harmonic generation (HHG) [20–22] and the orbital imaging with photoelectron spectroscopy, such as laser-induced electron diffraction (LIED) [23] and strong-field photoelectron holography (SFPH) [24]. The tomographic imaging method with HHG requires the measurement of the amplitude and phase of the high-order harmonics [20]. Whereas the amplitude of the HHG is easily measurable in experiment, the measurement of the phase is more challenging to access. In practice, the phase information of the high-order harmonics is obtained with theoretical calculations [20] or additional measurements [22]. In contrast, with our imaging method, the information of the relative phases between the constituent atomic orbitals is imprinted in the interference pattern of the PADs and can be extracted by fitting the interference fringes. On the other hand, orbital imaging with LIED assumes that there is only one atomic orbital for each nucleus of the molecule O_2 [23]. However, for common molecules, their molecular orbitals are usually composed of different types of atomic orbitals. Whether such molecular orbitals can be reconstructed with LIED is still unknown. Additionally, SFPH has been used to reconstruct the dynamics of the electron packet, e.g., valence electron motion of H_2^+ induced by the coherent superposition of two electronic states [24]. However, in this method, the molecular orbital of each electronic state is still obtained by solving the Schrödinger equation.

Experimental Design

The experiment is performed with cold-target recoil-ion momentum spectroscopy (COLTRIMS) [25,26] (for our apparatus, refer to our previous publications [27–29]). A linearly polarized femtosecond laser pulse is generated from a Ti:sapphire femtosecond laser system with a repetition rate of 5 kHz, a pulse duration of around 30 fs, and a center wavelength of 800 nm. The pulse passes through a β-BBO crystal to create two-color fields, which are then split into a stretched alignment pulse (800 nm, ~80 fs) and a probe pulse (400 nm, 35 fs). The two pulses are focused by an on-axis spherical mirror onto a cold supersonic gas jet of N_2 molecules inside the vacuum chamber of the COLTRIMS. The probe pulse, which is applied after a time delay, ionizes the molecules aligned by the alignment pulse. Any alignment angle of the molecule with respect to the polarization of the probe pulse can be achieved by rotating the alignment pulse polarization with a half-wave plate [30]. The alignment degree estimated from a two-dimensional (2D) angular distribution of ions by using the Coulomb explosion method [31,32] is about 0.79 at the time delay of 4.1 ps. We measure the 3D momenta of the produced photoelectrons in coincidence with the singly charged ions. The alignment pulse creates a low ionization background (<0.5%) compared to the ionization pulse. Through the fitting of the delay-dependent degree of alignment [31], we determine that the alignment pulse intensity is approximately 6.5×10^{13} W/cm^2, and the initial rotational temperature of the molecule is estimated to be approximately 50 K.

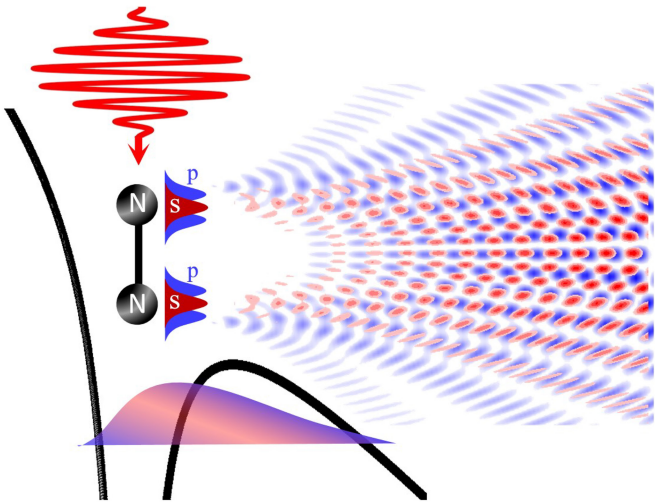

Fig. 1. Schematic view of the LETS. The electron of a molecule in HOMO can be ionized by tunneling through a barrier formed by the molecular potential and the laser electric field. According to the LCAO theory, the HOMO of N_2 is written as a linear combination of the 2*s* and 2*p* atomic orbitals for each core. The tunnel-ionized electron wavepackets from the 2*s* and 2*p* atomic orbitals interfere with each other, causing a modulation in the PADs. In addition, the electron wavepackets from the different cores exhibit a two-center interference.

Results and Discussion

In Fig. 2A and B, we present the measured PADs for the parallel and perpendicular alignments of the molecular N_2 with respect to the laser polarization, respectively. For momenta larger than 0.6 atomic units (a.u.), the PADs show a modulation, which is due to the intercycle interference patterns caused by the well-known above-threshold ionization [14]. Here, we will focus on the low-energy ($p < 0.6$ a.u.), radial fan-like patterns, which

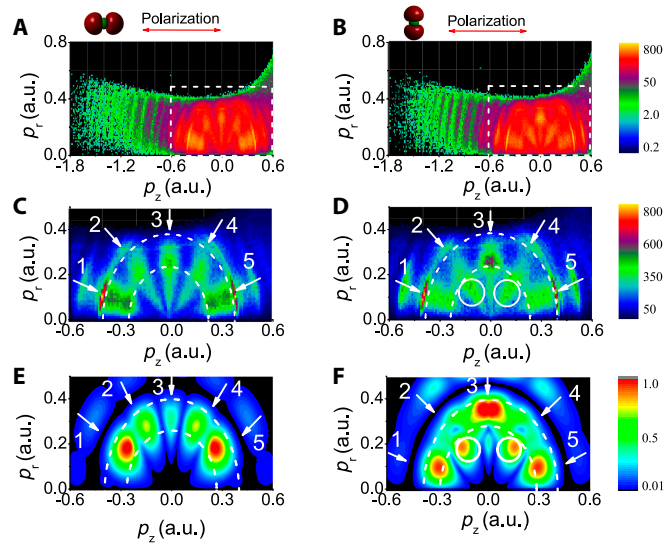

Fig. 2. (A and B) Experimental results for the parallel and perpendicular alignments of the molecular N_2 with respect to the laser polarization, respectively. The sketch above denotes the HOMO of the aligned N_2 and the laser polarization direction. p_z and p_r ($p_r = \sqrt{p_x^2 + p_y^2}$) represent the momenta parallel and perpendicular to the laser polarization axis, respectively. The data points with $p_r > 0.5$ a.u. are removed because of the influence of the spectrometer magnetic field. The laser intensity we used is $I = 2 \times 10^{14}$ W/cm^2 with the wavelength of 400 nm, which is in the tunneling ionization region. (C and D) Enlarged view of the measured PADs in the low-energy region marked by a rectangle in (A) and (B). (E and F) Simulated PADs with the M-CQSFA theory. For comparison to the experimental data, both the focal-averaged effect of the laser field and the alignment degree of the molecular axis are considered in our simulations.

are enlarged in Fig. 2C and D. There are five radial stripes for both parallel and perpendicular alignments. The radial stripes indicated by 1 and 5 exhibit a narrow peak at momentum $p = 0.4$ a.u., which is likely due to a Freeman resonance [33] (see the Supplementary Materials). Interestingly, for the parallel alignment, each stripe maximizes in the same energy band, indicated by the dashed white semi-circles. In contrast, for the perpendicular alignment, the second and fourth stripes maximize at lower energies.

To explain the experimental findings, we model the corresponding PADs. For an atomic system, we developed a Coulomb-corrected strong-field approximation (SFA) theory, coined as Coulomb quantum-orbit strong-field approximation (CQSFA) theory [34,35], to reproduce the fan-like patterns in the PADs [36,37]. Here, we extend our previous work and develop a molecular CQSFA (M-CQSFA) to help understand the alignment-dependent fan-like structures in our measurement. Briefly, the M-CQSFA theory is derived from the exact transition amplitude of an electron from a bound state $|\psi_0\rangle$ of a molecule to the continuum state $|\psi_{\boldsymbol{p}}(t)\rangle$ with drift momentum $\boldsymbol{p}$ [14]:

$$M(\boldsymbol{p}) = -i\lim_{t\to\infty}\int_{-\infty}^{t} dt' \left\langle \psi_{\boldsymbol{p}}(t)|U(t,t')H_I(t')|\psi_0(t')\right\rangle \quad (1)$$

where $H_I(t) = \boldsymbol{r}\cdot\boldsymbol{E}(t)$ is the interaction of a laser field with the electron and $U(t,t')$ is the time-evolution operator. In the framework of the LCAO theory [17,18], the initial state ψ_0 can be written as a weighted sum of the constituent atomic orbitals of each core. Furthermore, by employing the Feynman path integral formalism and the saddle-point approximation [34,35], the transition amplitude is written as:

$$M(\boldsymbol{p}) \propto -i\lim_{t\to\infty}\sum_{s}\left\{\det\left[\frac{\partial \boldsymbol{q}_s(t)}{\partial \boldsymbol{r}_s(t_{0,s})}\right]\right\}^{-1/2} e^{iS(\boldsymbol{q}_s,\boldsymbol{r}_s,t_{0,s},t)}$$

$$\times C(t_{0,s})\sum_{a}\left\langle \boldsymbol{q}_s(t_{0,s}) + \boldsymbol{A}(t_{0,s})\,|\,\mathbf{r}\cdot\boldsymbol{E}(t_{0,s})\,|\,\psi_a\right\rangle$$

$$\times c_a\left[e^{i\boldsymbol{p}\cdot\boldsymbol{R}/2} + (-1)^{l_a}e^{-i\boldsymbol{p}\cdot\boldsymbol{R}/2}\right], \quad (2)$$

where the index a denotes the different atomic orbitals, the index s represents the different quantum trajectories with the action $S(\boldsymbol{q}_s, \boldsymbol{r}_s, t_{0,s}, t)$, and l_a is the orbital quantum number of the atomic orbitals. In comparison with the CQSFA theory for atoms [34], there is an additional term: $e^{i\boldsymbol{p}\cdot\boldsymbol{R}/2} + (-1)^{l_a}e^{-i\boldsymbol{p}\cdot\boldsymbol{R}/2}$, corresponding to the two-center interference. In practice, the coefficients of the molecular orbital are obtained from quantum chemistry code [38]. In addition, numerous studies have revealed the multiple orbitals effect in the ionization of molecules [15]. However, it has been shown that the ionization probability from HOMO is still much larger than that from lower lying orbitals for any molecular alignment [39]. Hence, here, we focus solely on the ionization of the HOMO in N_2. Additionally, to facilitate comparison with experimental data, we incorporate the focal volume averaging present in the experiment and the experimentally achieved alignment degree (approximately 0.79) in our simulations.

Figure 2E and F shows the M-CQSFA-simulated PADs of the N_2 molecule for parallel and perpendicular alignments, respectively. In agreement with the experiment, our simulations also produce five radial stripes for both parallel and perpendicular alignments. In addition, for perpendicular alignment, the second and fourth radial stripes also shift to the low-energy band of the PAD (see the full white circles in Fig. 2F). Note that the pronounced intensity stripes from the Freeman resonance are absent in our simulations, because such a resonance process is neglected in our theoretical model.

Next, we use our simulation to explain the observed alignment dependence of the PAD. Figure 3 shows the PADs from the s and p orbitals in the HOMO of N_2 for the parallel and perpendicular alignments, respectively. We find that the low-energy shift of the second and fourth radial stripes shown in the total spectrum of Fig. 2F cannot be observed in Fig. 3B or D. This indicates that the low-energy shift of the radial stripes originates from the interference of the s and p orbital tunneling currents.

To further uncover the underlying physics of the low-energy shift of the radial stripes, we now analyze the relative phase between the transition amplitudes of the s and p orbitals in Eq. 2 (for more details, see the Supplementary Materials). By comparing the terms relevant to the atomic orbitals, we find that, for the perpendicular alignment, the relative phase is closely related to the combination coefficients c_a of the atomic orbitals in the LCAO theory. A calculation using a standard quantum chemistry package [38] shows that the combination coefficients for $2s$ and $2p$ are opposite in their signs, corresponding to a relative phase of π. Thus, in the total spectrum, the contributions of the s and p orbitals interfere destructively.

Figure 3B and D shows that the amplitudes of the second and fourth radial stripes between the two white dashed semi-circles are almost the same for the s and p orbitals. Therefore, the relative phase of π will lead to a substantial ionization suppression in the corresponding region of the total PAD. In the low-energy part of the second and fourth radial stripes, the s orbital has a higher probability than the p orbital. Thus, in the coherent sum of the photocurrent amplitudes from the s- and the p-orbitals, these two radial maxima will appear shifted to lower energy. In contrast, for the first, third, and fifth stripes, the relevant amplitudes of the s and p orbitals differ significantly, resulting in a weak interference between

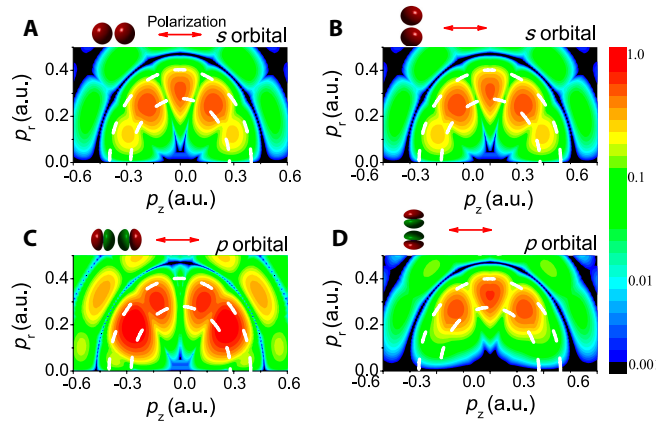

Fig. 3. M-CQSFA simulated PADs from the s orbitals (A and B) and the p orbitals (C and D) in the HOMO of N_2. Left column, parallel alignment; right column, perpendicular alignment.

them. Accordingly, these radial stripes retain their maxima in the higher energy region.

For the parallel alignment in Fig. 3A and C, our analysis shows that there is an additional term relevant to the initial momentum along the laser polarization in the transition amplitude of the *s* orbitals (for more details, see the Supplementary Materials). According to the saddle-point equations [14], the initial photoelectron momentum along the laser polarization is purely imaginary, and thus, the relative phase of the transition amplitudes of the *s* and *p* orbitals becomes $\pi/2$. In this case, the total spectrum is approximately equal to the direct sum of the contributions from the *s* and *p* orbitals shown in Fig. 3A and C.

In the following, we will demonstrate that the specific low-energy shift of the radial stripes for perpendicular molecular alignment determines the relative phases of the combination coefficients associated with the atomic orbitals, which provides a LETS-based method to reconstruct the molecular orbital in the framework of the LCAO theory. According to the LCAO theory [17,18], the molecular orbital can be written as a weighted sum of the constituent atomic orbitals of each core. For the nitrogen atom, there are three bound atomic orbitals: 1*s*, 2*s*, and 2*p*. Thus, the molecular orbital of N_2 can be generally written as

$$\psi_0(\boldsymbol{r}) \approx \sum\nolimits_{a=1s,2s,2p} |c_a| e^{i\theta_a} \left[\psi_a(\boldsymbol{r}+\boldsymbol{R}/2) + s_a \psi_a(\boldsymbol{r}-\boldsymbol{R}/2)\right], \quad (3)$$

where $|c_a|$ is the weighted coefficient with the phase of θ_a and the coefficient s_a is relevant to the symmetry of the molecular orbital. Recently, we have proposed and demonstrated a tomographic method to extract the value of $\boldsymbol{R}$ from the measured photoelectron momentum spectra of N_2 [29]. In this work, the combination coefficients ($|c_a|$, θ_a, s_a) for the molecular orbital are extracted by fitting the interference patterns in the PAD, while the wavefunction of each single nitrogen atom is calculated with a quantum chemistry code.

First, one needs to obtain the coefficient s_a from the data. The coefficient $s_a = (-1)^{l_a}$ for g symmetry of the molecular orbital, while $s_a = (-1)^{l_a+1}$ for u symmetry. If the molecular orbital has u symmetry, the ionization from the *s* orbital of the two cores will have a two-center interference term of $\sin(\boldsymbol{p}\cdot\boldsymbol{R}/2)$ [40], which leads to the ionization suppression for the photoelectron with $\boldsymbol{p} \perp \boldsymbol{R}$. On the other hand, for the *p* orbital along the molecular axis, due to its nodal structure, the ionization for the photoelectron with $\boldsymbol{p} \perp \boldsymbol{R}$ is also suppressed. Thus, in the total PAD, the ionization distribution of the photoelectron with $\boldsymbol{p} \perp \boldsymbol{R}$ will be vanishing. However, our measurement in Fig. 2C and D shows that there are clear ionization distributions for the photoelectron with $\boldsymbol{p} \perp \boldsymbol{R}$. This indicates that the HOMO of N_2 should have the g symmetry, and therefore, $s_a = (-1)^{l_a}$.

Next, we show how to extract the weighted coefficients $|c_a|$ and the phases θ_a of the different atomic orbitals from the measurements by fitting the PAD for the perpendicular alignment with our M-CQSFA theory. Usually, such fitting procedure is time-consuming for many coefficients. However, according to the LCAO theory, the combination coefficients are positive or negative real numbers, i.e., the phase θ_a is 0 or π. This will greatly simplify our fitting procedure. Additionally, because the 1*s* atomic orbital is tightly bound, its ionization amplitude can be neglected in our case. For simplicity, we set $c_{1s} = 0$ in our calculation. Thus, we consider only the linear combination of the 2*s* and 2*p* atomic orbitals, and vary the ratio of $|c_{2s}|/|c_{2p}|$ and their relative phase in our fitting procedure. Our simulation

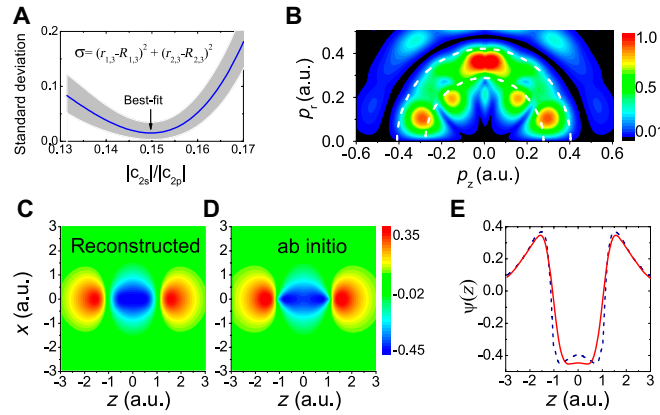

Fig. 4. (A) Standard deviation of the relative amplitudes of the different interference stripes between the measurement and the simulation as a function of the ratio of $|c_{2s}|/|c_{2p}|$. The shaded area surrounding the solid line is related to the statistical uncertainty of the amplitude ratios ($R_{1,3}$ and $R_{2,3}$) associated with the measurement. In our fitting procedure, the focal-averaged effect of the laser field and the alignment degree of the molecular axis are considered. (B) M-CQSFA-simulated PAD for the perpendicular alignment with the best-fit ratio. (C) Reconstructed molecular orbital wavefunction of N_2 with the best-fit ratio. (D) Shape of the molecular orbital from an ab initio calculation. (E) Cuts along the molecular axis for the reconstructed (solid) and ab initio (dashed) wavefunctions.

result shows that, when the relative phase is π, the low-energy shift of the second and fourth radial stripes in the measurement can be approximately reproduced. To obtain the best-fit ratio of $|c_{2s}|/|c_{2p}|$, we analyze the relative amplitude of the five radial stripes of the fan-like patterns. To simplify the analysis, we take the third radial stripe as a reference point and calculate the ratio between the first and third radial stripes $r_{1,3} = A_1/A_3$ and the ratio between the second and third radial stripes $r_{2,3} = A_2/A_3$. Here, A_i ($i = 1$, 2, and 3) denotes the integrated ionization amplitude of the different radial stripes. To compare our results with the measured PADs, we obtain the corresponding ratios ($R_{1,3}$ and $R_{2,3}$) from the experimental data. By calculating the difference between the calculated and measured ratios, $\sigma = (r_{1,3} - R_{1,3})^2 + (r_{2,3} - R_{2,3})^2$, we quantify the discrepancy between the simulation and measurement. In Fig. 4A, we present this difference as a function of the $|c_{2s}|/|c_{2p}|$ ratio. Notably, the value of σ is minimized when the ratio is approximately 0.1495, indicating that the simulated amplitude distribution of the five radial stripes closely matches the experimentally measured result. Moreover, we also consider the statistical uncertainty associated with our measurement. In our experiment, we obtained multiple sets of photoelectron spectra for each molecular axis. The amplitude ratios, $R_{1,3}$ and $R_{2,3}$, of these spectra were analyzed to determine their corresponding statistical uncertainties: $\Delta R_{1,3}$ and $\Delta R_{2,3}$. These uncertainties are taken into account in the calculation of the difference σ, which is visually represented by the shaded area surrounding the solid line in Fig. 4A.

In Fig. 4B, we show the M-CQSFA-simulated PAD for the perpendicular alignment with the best-fit ratio, which agrees well with the measurement in Fig. 2D and the simulation in Fig. 2F. In Fig. 4C, we present the reconstructed electron wavefunction of the HOMO of N_2 according to Eq. 3 with the best-fit ratio of 0.1495 and a relative phase of π between 2*s* and 2*p*. One can see that the reconstructed wavefunction is well consistent with the ab initio orbital calculation of the N_2 shown in Fig. 4D. The minor difference of the electron wavefunction near the two cores ($z = \pm R/2 \sim \pm 1$ a.u.) (see Fig. 4E) is due to the neglect

of the tightly bound 1*s* atomic orbital in our fitting algorithm. A similar difference in the reconstructed wavefunction, relevant to the 1*s* atomic orbital, is also present in the molecular-orbital tomography with HHG [20].

Conclusion

In summary, we have proposed and experimentally demonstrated a method to reconstruct the molecular orbital in the framework of LCAO based on LETS. Using the example of the N_2 molecule, we have observed a specific interference pattern in PADs for perpendicular molecular alignment, which is used to successfully extract the weighted coefficients and the relative phase of the constituent atomic orbitals for the HOMO of N_2. For larger molecules, the strong-field ionization will lead to the appearance of more relevant peculiar features in the PADs (an example can be found in the Supplementary Materials), which will benefit the accurate reconstruction of more complicated molecular orbitals with our imaging method. In addition, if combined with a conventional pump-probe scheme, it should be possible to detect the evolution of molecular orbitals in real time and to observe electronic rearrangement during a photochemical reaction. The derived information of the constituting atomic orbitals will provide a comprehensive understanding of the molecular dynamics.

Acknowledgments

Funding: This work is supported by the National Key Program for S&T Research and Development (grant no. 2019YFA0307702), the National Natural Science Foundation of China (grant nos. 11834015, 11922413, 12121004, 12274420, and 12004394), the Strategic Priority Research Program of the Chinese Academy of Sciences (grant no. XDB21010400), CAS Project for Young Scientists in Basic Research (grant no. YSBR-055), the Science and Technology Department of Hubei Province (grant nos. 2020CFA029 and 2021CFA078), and K.C. Wong Education Foundation.

Author contributions: X.L., A.S., and X.L. conceived and designed the work. R.S., S.Y., and W.Q. performed the experiments. X.L. and Y.W. built the theoretical codes and performed the calculations. X.L., R.S., Y.W., A.S., and X.L. performed analysis and interpreted the data. The manuscript was prepared by X.L., A.S., and X.L. and was discussed among all authors.

Competing interests: The authors declare that they have no competing interests.

Data Availability

The data that support the plots within this paper and other findings of this study are available from the corresponding author upon reasonable request.

Supplementary Materials

Supplementary Text
Figs. S1 to S3

References

1. Pauling L. *The nature of the chemical bond and the structure of molecules and crystals*. Ithaca (New York): Cornell University Press; 1960.
2. Mohn F, Gross L, Moll N, Meyer G. Imaging the charge distribution within a single molecule. *Nat Nanotechnol*. 2012;7:227.
3. Cocker TL, Peller D, Yu P, Repp J, Huber R. Tracking the ultrafast motion of a single molecule by femtosecond orbital imaging. *Nature*. 2016;539(7628):263–267.
4. Puschnig P, Berkebile S, Fleming AJ, Koller G, Emtsev K, Seyller T, Riley JD, Ambrosch-Draxl C, Netzer FP, Ramsey MG. Reconstruction of molecular orbital densities from photoemission data. *Science*. 2009;326(5953):702–706.
5. Frietsch B, Carley R, Döbrich K, Gahl C, Teichmann M, Schwarzkopf O, Wernet P, Weinelt M. A high-order harmonic generation apparatus for time- and angle-resolved photoelectron spectroscopy. *Rev Sci Instrum*. 2013;84(7):Article 075106.
6. Puschnig P, Reinisch EM, Ules T, Koller G, Soubatch S, Ostler M, Romaner L, Tautz FS, Ambrosch-Draxl C, Ramsey MG. Orbital tomography: Deconvoluting photoemission spectra of organic molecules. *Phys Rev B*. 2011;84:Article 235427.
7. Meckel M, Comtois D, Zeidler D, Staudte A, Pavičić D, Bandulet HC, Pépin H, Kieffer JC, Dörner R, Villeneuve DM, et al. Laser-induced electron tunneling and diffraction. *Science*. 2008;320(5882):1478–1482.
8. Kübel M, Dube Z, Naumov AY, Villeneuve DM, Corkum PB, Staudte A. Spatiotemporal imaging of valence electron motion. *Nat Commun*. 2019;10:1042.
9. Murray R, Spanner M, Patchkovskii S, Ivanov MY. Tunnel ionization of molecules and orbital imaging. *Phys Rev Lett*. 2011;106(17):Article 173001.
10. Wollenhaupt M, Engel V, Baumert T. Femtosecond laser photoelectron spectroscopy on atoms and small molecules: Prototype studies in quantum control. *Annu Rev Phys Chem*. 2005;56:25–56.
11. Grasbon F, Paulus GG, Chin SL, Walther H, Muth-Böhm J, Becker A, Faisal FHM. Signatures of symmetry-induced quantum-interference effects observed in above-threshold ionization spectra of molecules. *Phys Rev A*. 2001;63:041402(R).
12. Holmegaard L, Hansen JL, Kalhøj L, Louise Kragh S, Stapelfeldt H, Filsinger F, Küpper J, Meijer G, Dimitrovski D, Abu-samha M, et al. Photoelectron angular distributions from strong-field ionization of oriented molecules. *Nat Phys*. 2010;6:428–432.
13. Keldysh LV. Ionization in the field of a strong electromagnetic wave. *J Exp Theor Phys*. 1965;47(5):1945.
14. Becker W, Grasbon F, Kopold R, Milošević DB, Paulus GG, Walther H. Above-threshold ionization: From classical features to quantum effects. *Adv At Mol Opt Phys*. 2002;48:35–98.
15. Akagi H, Otobe T, Staudte A, Shiner A, Turner F, Dörner R, Villeneuve DM, Corkum PB. Laser tunnel ionization from multiple orbitals in HCl. *Science*. 2009;325:1364–1367.
16. Xie X. Two-dimensional attosecond electron wave-packet interferometry. *Phys Rev Lett*. 2015;114(17):Article 173003.
17. Hückel E. Quantentheoretische beiträge zum benzolproblem. *Z Physik*. 1931;70:204–286.
18. Lennard-Jones JE. The electronic structure of some diatomic molecules. *Trans Faraday Soc*. 1929;25:668–686.
19. Poudel L, Steinmetz NF, French RH, Parsegian VA, Podgornik R, Ching W-Y. Implication of the solvent effect, metal ions and topology in the electronic structure and hydrogen bonding of human telomeric G-quadruplex DNA. *Phys Chem Chem Phys*. 2016;18(31):21573–21585.

20. Itatani J, Levesque J, Zeidler D, Niikura H, Pépin H, Kieffer JC, Corkum PB, Villeneuve DM. Tomographic imaging of molecular orbitals. *Nature*. 2004;432:867–871.
21. Haessler S, Caillat J, Boutu W, Giovanetti-Teixeira C, Ruchon T, Auguste T, Diveki Z, Breger P, Maquet A, Carré B, et al. Attosecond imaging of molecular electronic wave-packets. *Nat Phys*. 2010;6:200–206.
22. Bertrand JB, Wörner HJ, Salières P, Villeneuve DM, Corkum PB. Linked attosecond phase interferometry for molecular frame measurements. *Nat Phys*. 2013;9:174–178.
23. Puthumpally-Joseph R, Viau-Trudel J, Peters M, Nguyen-Dang TT, Atabek O, Charron E. Inversion of strong-field photoelectron spectra for molecular orbital imaging. *Phys Rev A*. 2016;94: Article 023421.
24. He MR, Li Y, Zhou YM, Li M, Cao W, Lu PX. Direct visualization of valence electron motion using strong-field photoelectron holography. *Phys Rev Lett*. 2018;120(13):Article 133204.
25. Dörner R, Mergel V, Jagutzki O, Spielberger L, Ullrich J, Moshammer R, Schmidt-Böcking H. Cold target recoil ion momentum spectroscopy: A 'momentum microscope' to view atomic collision dynamics. *Phys Rep*. 2000;330:95–192.
26. Ullrich J, Moshammer R, Dorn A, Dörner R, Ph L, Schmidt H, Schmidt-Böcking H. Recoil-ion and electron momentum spectroscopy: Reaction-microscopes. *Rep Prog Phys*. 2003;66(9):1463.
27. Wang YL, Xu SP, Quan W, Gong C, Lai XY, Hu SL, Liu MQ, Chen J, Liu XJ. Recoil-ion momentum distribution for nonsequential double ionization of Xe in intense midinfrared laser fields. *Phys Rev A*. 2016;94:Article 053412.
28. Quan W, Hao XL, Hu XQ, Sun RP, Wang YL, Chen YJ, Yu SG, Xu SP, Xiao ZL, Lai XY, et al. laser-induced inelastic diffraction from strong-field double ionization. *Phys Rev Lett*. 2017;119(24):Article 243203.
29. Sun RP, Lai XY, Yu SG, Wang YL, Xu SP, Quan W, Liu XJ. Tomographic extraction of the internuclear separation based on two-center interference with aligned diatomic molecules. *Phys Rev Lett*. 2019;122(19):Article 193202.
30. Meckel M, Staudte A, Patchkovskii S, Villeneuve DM, Corkum PB, Dörner R, Spanner M. Signatures of the continuum electron phase in molecular strong-field photoelectron holography. *Nat Phys*. 2014;10:549–600.
31. Dooley PW, Litvinyuk IV, Lee KF, Rayner DM, Spanner M, Villeneuve DM, Corkum PB. Direct imaging of rotational wave-packet dynamics of diatomic molecules. *Phys Rev A*. 2003;68:Article 023406.
32. Pavičić D, Lee KF, Rayner DM, Corkum PB, Villeneuve DM. Direct measurement of the angular dependence of ionization for N_2, O_2, and CO_2 in intense laser fields. *Phys Rev Lett*. 2007;98(24):Article 243001.
33. Freeman RR, Bucksbaum PH, Milchberg H, Darack S, Schumacher D, Geusic ME. Above-threshold ionization with subpicosecond laser pulses. *Phys Rev Lett*. 1987;59:1092.
34. Lai XY, Poli C, Schomerus H, Figueira de Morisson Faria C. Influence of the coulomb potential on above-threshold ionization: A quantum-orbit analysis beyond the strong-field approximation. *Phys Rev A*. 2015;92:Article 043407.
35. Maxwell AS, Figueira de Morisson Faria C. It is all about phases: Ultrafast holographic photoelectron imaging. *Rep Prog Phys*. 2020;83:Article 034401.
36. Maharjan CM, Alnaser AS, Litvinyuk I, Ranitovic P, Cocke CL. Wavelength dependence of momentum-space images of low-energy electrons generated by short intense laser pulses at high intensities. *J Phys B*. 2006;39(8):1955.
37. Shvetsov-Shilovski NI, Lein M, Madsen LB, Räsänen E, Lemell C, Burgdörfer J, Arbó DG, Tőkési K. Semiclassical two-step model for strong-field ionization. *Phys Rev A*. 2016;94:Article 013415.
38. Frisch MJ, Trucks GW, Schlegel HB, Scuseria GE, Robb MA, Cheeseman JR, Scalmani G, Barone V, Mennucci B, Petersson GA, et al. *GAUSSIAN 09 (Revision D.01)*. Wallingford (CT): Gaussian Inc.; 2013.
39. Petretti S, Vanne YV, Saenz A, Castro A, Decleva P. Alignment-dependent ionization of N_2, O_2, and CO_2 in Intense Laser Fields. *Phys Rev Lett*. 2010;104(22):Article 223001.
40. Busuladžić M, Gazibegović-Busuladžić A, Milošević DB, Becker W. Angle-resolved high-order above-threshold ionization of a molecule: Sensitive tool for molecular characterization. *Phys Rev Lett*. 2008;100(20):Article 203003.